CHINESE OPTICS LETTERS

Vol. 20, No. 7 | July 2022

Rabi antenna using microstrip add-drop multiplexer for electron warp speed investigation

Somchat Sonasang[1], Prakasit Prabpal[2], Piya Sirikan[2], Pratimakorn Hakaew[2], Nhat Truong Pham[3,4], Preecha Yupapin[2], Kanad Ray[5,6,7], and Sarawoot Boonkirdram[8*]

[1] Department of Electronic Technology, Faculty of Industrial Technology, Nakhon Phanom University, Nakhon Phanom 48000, Thailand

[2] Department of Electrical Technology, School of Industrial Technology, Sakonnakhon Technical College, Institute of Vocational Education Northeastern Region 2, Sakonnakhorn 47000, Thailand

[3] Division of Computational Mechatronics, Institute for Computational Science, Ton Duc Thang University, Ho Chi Minh City 72915, Vietnam

[4] Faculty of Electrical and Electronics Engineering, Ton Duc Thang University, Ho Chi Minh City 72915, Vietnam

[5] Amity School of Applied Sciences, Amity University Rajasthan, Jaipur, India

[6] Faubert Lab, Université de Montréal, H3T 1P1 Montréal, Canada

[7] Facultad de CienciasFisico-Matematicas, Benemérita Universidad Autónoma de Puebla, Av. San Claudio y Av. 18 sur, Col. San Manuel Ciudad Universitaria, Puebla Pue 72570, Mexico

[8] Program of Electrical and Electronics, Faculty of Industrial Technology, Sakon Nakhon Rajabhat University, Sakon Nakhon 47000, Thailand

*Corresponding author: sarawoot.b@snru.ac.th

Received December 13, 2021 | Accepted April 24, 2022 | Posted Online May 31, 2022

This work presents experimental results of Rabi antenna characteristics using the coupled line microstrip circuit. It was constructed by a modified coupled line microstrip four-port network, which is known as an add-drop multiplexer. The driven AC input enters the device via an input port using the suitable frequency and coupled line microstrip ring radius. The multi-level system is generated by a wave-particle aspect before the two-level system is achieved. At the resonance, the transitions of the states induce the energy called whispering gallery mode (WGM) at the circuit center, which is the squeezed energy. The generated electron oscillation within the WGM envelope oscillated by the frequency is known as the Rabi frequency. By the successive filtering with continuous AC input via the selected port, the electron cloud warp speed can be generated and achieved inside the two-level transition. The constructed microstrip ring radius is 25 mm, and the experimental results of the Rabi antenna characteristics are in good agreement with the simulation results. The obtained resonant antenna oscillation frequency is 2.103 GHz. The electron cloud warp speed of 1.100c and time dilation of 0.006 μs are obtained.

Keywords: integrated photonics; waveguide; microwave photonics; Rabi antenna.
DOI: 10.3788/COL202220.073901

1. Introduction

Optical Rabi vibration is a basic example of coherent nonlinear light–material interaction[1–7]. In the case of eigen transitions such as excitons of semiconductors, the same situation can be seen in solids in principle. The solid Rabi vibration acts as a solid coherent control. Attempts to establish exciton Rabi cycles indicate their existence. However, in banded semiconductor structures, rapid phase relaxation makes exciton coherent control more difficult. In recent years, Rabi splitting has been of great interest in studying the interaction effects of matter and electromagnetic waves[8–12]. When an atomic two-level system, with considerable exciton resonance is introduced inside the microcavity, the coupling between the two-level transitions because of resonance and the cavity mode causes Rabi splitting and Rabi vibration. In the bonded atomic cavity system, two transmission peaks and two reflection drops are seen. Rabi vibration can visibly illustrate the discrete character of coherent energy exchange between atoms and electromagnetic fields. Coherent manipulation of a single two-stage quantum arrangement by means of electromagnetic fields by adjusting the amplitude, frequency, and envelope curve of the electromagnetic field is the basic tool of quantum optics. Resonant photon–atom interactions support exciting phenomenon like the Rabi cycle. It is ubiquitous in quantum information technology and is extensively used in the initialization, manipulation, and measurement of qubits in various physical systems.

Kuruma *et al.*[13] implemented photonic crystal nanocavities with very high *Q* factors over 80,000 and used simple photoluminescence-based experiments to unambiguously resolve ultra-fast vacuum Rabi oscillations. Gudmundsson *et al.*[14] theoretically modeled time-dependent transmission through asymmetric double quantum dots etched into 2D wires embedded in photonic resonators in the far-infrared (FIR) region. Wu *et al.*[9] proposed the Rydberg antiblockade (RAB) regime, in which Rabi oscillations amid the collective excited and ground states are induced. Soysouvanh *et al.*[15] recommended the employment of soliton pulses propagating inside a modified add-drop filter prepared by GaAsInP/P material. The shape is of a panda ring resonator, where the dark/bright soliton pulses are made as input to the system through the input port. The alteration between dark and bright soliton pulses is introduced with a 3 dB coupler with phase change of $\frac{\pi}{2}$. The output solitons received on the through and drop ports are bright and dark solitons, respectively. Both signals can be used to form "on" and "off", or "1" and "0." These are applicable for generating digital bits. Secure output bits can be placed in the application using alternate input solitons or control ports. The control port can convert bright and dark input solitons to output bits. It indicates that the output bit can be arbitrarily switched between "1" and "0." In addition, additional information is multiplexed through the additional port and sent over the whispering gallery mode (WGM) and over the port output over free space or fiber optics.

A silicon-based reconfigurable optical add-drop multiplexer (ROADM) has been announced for hybrid wavelength and mode multiplexing systems[16]. Naghdi and Chen[17] demonstrated a compact photonic four-channel optical add-drop multiplexer (OADM) made of silicon. This is made possible by a reverse coupler based on a sub-wavelength grating. Saber *et al.*[18] experimentally investigated an ultra-compact single-stage and cascade OADM using misaligned sidewall Bragg gratings on a Mach–Zehnder interferometer for silicon isolator platforms. Wang *et al.*[19] proposed and demonstrated an integrated ROADM for time division multiplexing systems. Wu *et al.*[20] reported a reconfigurable four-channel OADM for use in access networks. The OADM was based on a vertically coupled thermal tunable Si_3N_4–SiO_2 microring resonator. Miller[21] showed how to extract the spatial mode from the light beam. This leaves the other orthogonal modes unaffected and allows us to retransmit new signals in this mode. An integrated eight-channel OADM with a cascaded upper sub-microring resonator has been experimentally demonstrated on a silicon on insulator (SOI) substrate.

Through thermoregulation, each channel can be independently switched between the add and drop states[22]. Kato *et al.*[23] proposed an additional tunable multiplexer in a silicon waveguide Mach–Zehnder interferometer with a sampled lattice structure and a ferroelectric liquid crystal (FLC) coating, which they fabricated. Multicore fiber optic couplers have been proposed to extract one of the modes in an optical fiber of several modes from the light beam, leaving the other modes free from interference and allowing a new signal to be retransmitted in this mode[24]. Pérez-Galacho *et al.*[25] recommended a mode-division multiplexing (MDM) insert/extractor for the first and second modes covering the entire C-band range. The instrument is based on the Mach–Zehnder interferometer.

In the present paper a two-stage system with a modified four-port circuit has been designed and proven. This system is formed by a modified four-port microstrip network. During operation, two energy states (frequency) are generated in the system. The state transition induced energy in the center of the circuit. This is called WGM. The electron cloud generated in the WGM shell oscillates at the Rabi frequency known as the Rabi antenna. Any wave-particle projection can form the Rabi oscillation. However, the Rabi oscillation can be formed when the speed of light is *c*, which means at the edge of the entangled pair of the two-level system. The multi-level system cannot form the Rabi oscillation. Therefore, the multi-level system is required to filter to have a pure two-level system. Then, the Rabi oscillation will occur. In this work, the filtering circuit is an add-drop multiplexer. The AC signal is made as input to the circuit formed by a nonlinear material. Initially, the multi-level system of the wave-particle is introduced. By using the successive filtering, the two-level system can be achieved. Hence, the system oscillated under the Rabi oscillation.

2. Theoretical Background

The structure of the parallel microstrip transmission line consists of a strip and parallel coupled lines[26]. The microstrip is designed as a microwave substrate with the relative dielectric constant in the microstrip, while air is above the two transmission lines with a dielectric constant (ε_0). In addition, a metal plate is under the microwave base material acting as the ground plane. Typically, a parallel coupled line microstrip has a paralleled span of approximately a quarter of the wavelength travelled on the transmission line ($\frac{\lambda_g}{4}$). The parallel coupled line microstrip consists of an input port (input, port 1), a connection port (coupled, port 2), an isolated port (isolation, port 3), and a through port (through, port 4), as shown in Fig. 1. Electrically

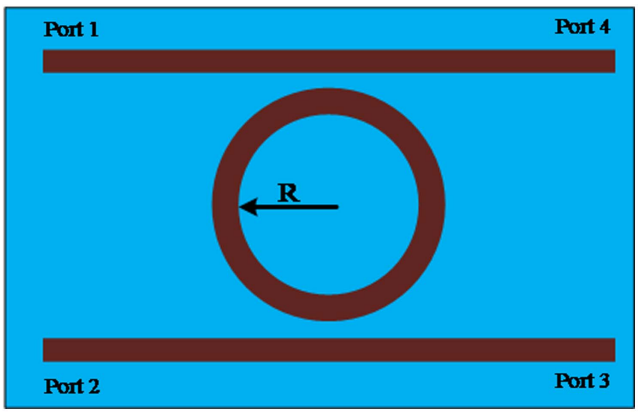

Fig. 1. Circuit structure. Port 1 is the location of E_{in}, Port 2 is the location of E_{dr}, Port 3 is the location of E_{add}, and Port 4 is the location of E_{th}.

in conjunction with network theory, considering that the characteristic impedance of the parallel coupled line microstrip is symmetrical, it is correlated by scattering parameter (S-parameter) according to the equation[27]

$$S_{ij} = 20 \log \frac{v_i}{v_j}, \tag{1}$$

where S_{ij} is the S-parameter, v_i indicates the output electrical signal (output), and v_j indicates electrical signal input (input). The parameter represents the proportion of electrical signal output and input. The ability to transmit electrical power from port 1 to port 2 is expressed by $S_{21} = 20 \log \frac{v_2}{v_1}$. In this article, the coupling factor of the parallel coupled line microstrip is less than −60 dB. The middle connection of the ring circuit assists the coupling of the wave signal from port 1 to port 2 and port 3. The resonant frequency band of the ring with a diameter size can apply to adopt the characteristics of a parallel coupled line microstrip in microstrip add-drop circuits, which is capable of circuit design with simple techniques due to its planar structure.

The AC source is made as input to the microstrip add-drop multiplexer circuit, as shown in Fig. 2. The electrons in the conductor are excited and oscillated. The electron plasma is formed and given by the Drude model[28] given in Eq. (2):

$$\varepsilon(\omega) = 1 - \frac{n_e e^2}{\varepsilon_0 m \omega^2}, \tag{2}$$

where n_e, e, ε_0, and m are the electron density, electron charge, permittivity of free space, and mass of electron, respectively. ω is the angular frequency. The plasma frequency is given by

$$\omega_p = \sqrt{\frac{n_e e^2}{\varepsilon_0 m}}. \tag{3}$$

Under successive filtering, the output resonance of the four-port network circuit in terms of the add-drop filter is given in Eqs. (4) and (5) as[29]

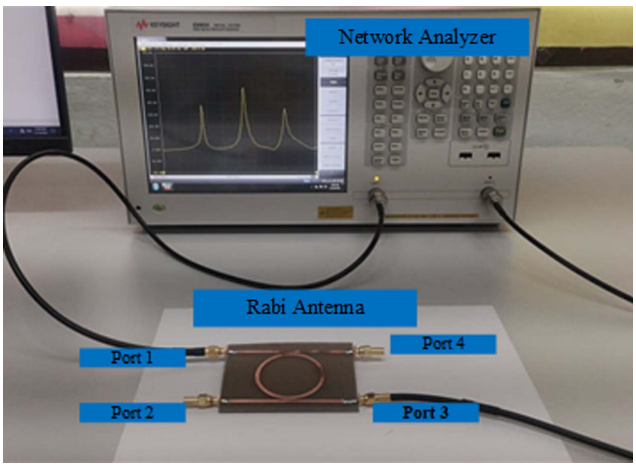

Fig. 2. Experimental setup.

$$E_{\text{th}} = m_2 E_{\text{in}} + m_3 E_{\text{add}}, \tag{4}$$

$$E_{\text{dr}} = m_5 E_{\text{add}} + m_6 E_{\text{in}}, \tag{5}$$

where the terms m_2, m_3, m_5, and m_6 are constants and explained in Ref. [29]. The normalized outputs are given in Eqs. (6) and (7):

$$I_{\text{th}} = I_{\text{in}} \left(\frac{E_{\text{th}}}{E_{\text{in}}} \right)^2, \tag{6}$$

$$I_{\text{dr}} = I_{\text{in}} \left(\frac{E_{\text{dr}}}{E_{\text{in}}} \right)^2, \tag{7}$$

where I_{in}, I_{th}, and I_{dr} are the input, through, and drop port electric field intensities, respectively.

A current source is made as input to a microstrip add-drop filter with a center frequency (f). When the system has undergone Rabi oscillation[16], the orthogonal (entangled) outputs are randomly detected by drop and through ports, respectively. A microstrip ring radius R and material refractive index n are used. The entangled photons are apart with a $\frac{\pi}{2}$ radian, which is the shortest distance of the wave-particle projection. The photon is first generated here, which is why the speed of light is constant in vacuum. It is also the origin of time.

Within a circular motion, the particle velocity is given by $v = \omega R$, where $\omega = 2\pi f$, and Δt from the measurement is $\frac{1}{\Delta f}$. The warp drive force (F_D) is given by

$$F_D = M_D \pi^2 f_D R_D, \tag{8}$$

where M_D is the total launching mass; $f_D = 4f^2$ is the driving frequency; R_D is the warp drive ring radius.

In general, the input AC source with the applied frequency (f) is fed into the input port, where it is modulated by the same frequency via an add port with the difference in phase of $\pm\Delta t$, which yields

$$e^{\pm i 2\pi f (t \pm \Delta t)}. \tag{9}$$

The travelling time of $\pm\Delta t$ is the required destination of the travelling, which can be obtained when the system is under the free running operation ($t = 0$).

3. Experiment and Results

In this work, we have applied the wave-particle aspect of the signals propagating within a photonic device. From Fig. 1, many particles move along the circular ring leading to a multi-level system before the two-level system arrives by successive filtering. The successive filtering means continuously running the input AC source into the add-drop filter, which has been clarified as the filtering device as given reference works. The matching ring radius and driven AC frequency are applied to obtain the Rabi oscillation. After successive filtering, the higher frequency leads to having the particle speed faster than light speed. The

plot between the microstrip ring radius and frequency has been shown in Fig. 3. From the matching between the Rabi frequency and ring radius to obtain the Rabi oscillation, where the speed of particles along the circular path is equal to c, 25 mm is the matching ring radius. The base used is FR4 material. When the displacement of two particles' travelling path is less than 1.5×10^{-14} m, the weak, electromagnetic, and strong coupling can be generated. Black holes (wormholes) can be also generated under successive filtering when the coupling effect has been established.

A new way of two-level system phenomenon behavior can be accommodated by the wave-particle moving along the circular motion, which can be used to form the Rabi oscillation in both theory and experiment. In this work, the antenna was formed by a parallel coupled line microstrip four-port network, where the coupling between the ring and waveguide structure can be used the same as an add-drop multiplexer. The circular part motion is formed by a modified microstrip add-drop multiplexer, as shown in Fig. 2. The prototype circuit used the microstrip add-drop multiplexer with substrate FR4, which has the following electrical properties: relative dielectric constant of 4.55, base material height of 1.60 mm, and tangent loss of 0.02. The program used is Sonnet Lite. The simulation was performed based on the electromagnetic waves effect of the microstrip add-drop multiplexer circuit to determine the response frequencies of the device using the momentum method. The results were obtained using a vector network analyzer (Keysight Network Analyzer model E5063A), where a reference-level network analyzer was used before the measurement. The measured frequencies were ranged from 100 kHz–4 GHz. The Rabi antenna design and simulation were applied to confirm the expected results before the construction, where the concept is that the Rabi oscillation can be formed by the add-drop multiplexer, from which the applied AC source with the specified frequency was fed into the add-drop multiplexer. The electrons (particles) were coupled and moved along the circular part under the successive filtering. The relationship between the current driving frequency and microstrip ring radius with the light speed c was calculated and plotted, as shown in Fig. 3(a). The condition was that the speed of light within the two-level transition gap was equal to the speed of light in a vacuum. The obtained result has shown that the AC driving frequency was related to the center ring radius, from which the suitable values were used in the experiment. Using the Drude equation, the relationship between the distributed photons and electron densities can be obtained. To obtain the electron speed faster than light speed, the Rabi oscillation is running successively to obtain the required resonant frequency.

From Fig. 2, the suitable microstrip ring radius and driven frequency source were selected and used as inputs into the microstrip add-drop multiplexer. The wave-particle aspect of the driven electromagnetic wave propagation within a nonlinear microstrip ring resonator is established, as shown in Fig. 3(b). The harmonic oscillator of two masses generated in the Rabi oscillation can be found in Ref. [30], where a clear description is given. In operation, the multi-level energy modes are initially formed and oscillated within the system, from which the higher-order energy modes of photon propagation in the system can be filtered by successive filtering within an add-drop device. Using the successive filtering continuously, the two-level system will be collapsed and stopped eventually, which will return again under the successive filtering. In the experiment, the speed of the moving particles equals the speed of light in a vacuum. The Rabi frequency is generated and observed. During the Rabi oscillation, the transition energy between the excited and ground states is the squeezed energy in the form of the WGM. Figure 4 shows the result of the Rabi oscillation obtained from the simulation using the system in the experiment, where the suitable ring radius is 25 mm when the resonant frequency is approximated to 2.103 GHz. Figure 4 shows the simulation results of the Rabi antenna response frequencies of f_1, f_0, f_2 and the coupling coefficients at the drop port (S_{21}) are 1.040, 2.103, 3.136 GHz and −16.733, −17.375, −18.051 dB, respectively. The add-port (S_{31}) results of the Rabi antenna response frequencies of f_1, f_0, f_2 and the connection coefficients are 1.040, 2.103, 3.136 GHz and −19.736, −17.350, −18.705 dB, respectively. The Rabi antenna response frequencies of f_1, f_0 and f_2 and normalized magnitudes at the drop port are 1.040, 2.103, 3.136 GHz and 0.145, 0.135, 0.125 according to Fig. 5(a), respectively. The simulated Rabi antenna response frequencies of f_1, f_0, f_2 and normalized magnitudes at the add port are 1.040, 2.103, 3.136 GHz and 0.103, 0.136, 0.166, as shown in Fig. 5(b), respectively. The

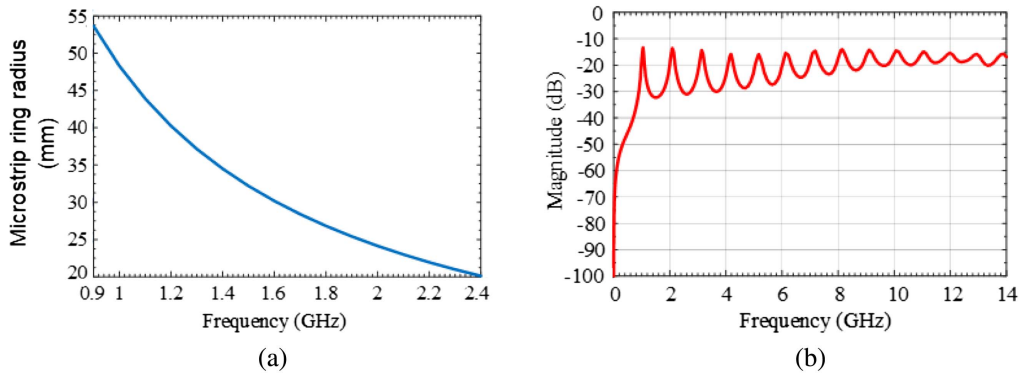

Fig. 3. (a) Plot between the microstrip ring radius and frequency and (b) the Rabi oscillation obtained from the experiment using the system.

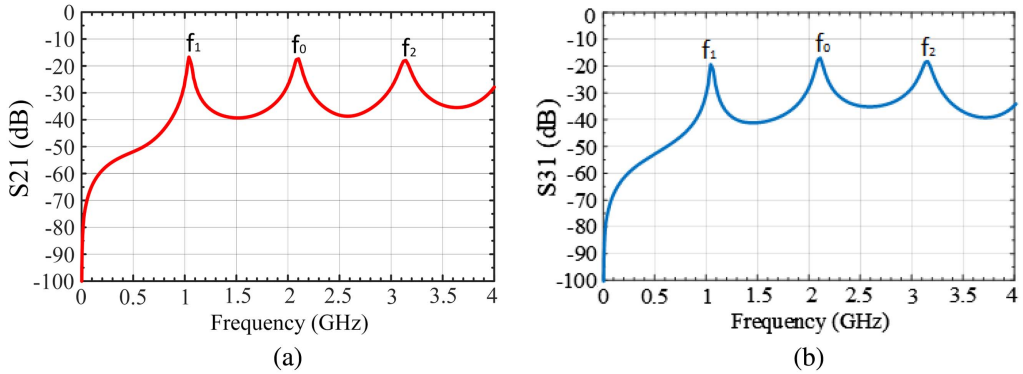

Fig. 4. Simulation frequency response of (a) S_{21} and (b) S_{31} of the Rabi antenna.

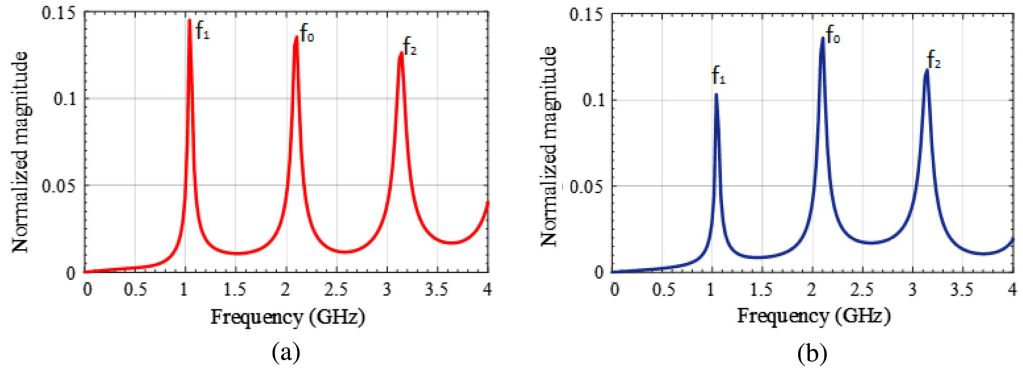

Fig. 5. Simulation of magnitude of (a) S_{21} and (b) S_{31} of the Rabi antenna.

different frequencies of f_0–f_1, f_2–f_0, f_2–f_1 are 1.033, 1.063, 2.096 GHz, respectively. The time domain of the Rabi antenna domain is shown in Fig. 6(a). The time domain obtained from the drop-port gap is −0.42713 (red line), while the time-domain response of an add port has a gap of 0.33214 (blue line) with a time difference of 0.006 μs (between 10.000 and 10.006 μs), as shown in Fig. 6(b), respectively. The blue- and red-shifts are generated from add and drop ports after the system undergoes successive filtering for 10 μs, as shown in Fig. 6(b), which indicates that the center envelope has a speed faster than light speed in a vacuum, which is calculated and is equal to 1.10c. The blue- and red-shifts can be configured as the fast and slow light pulses with respect to the center peak. The travelling photon is in one dimension with two sides of times (frequencies) generated by the Rabi oscillation. The center peak pulse width is 0.006 μs. In Fig. 7(a), the frequency response measurement results with the instruments presented previously show that the Rabi antenna frequencies of f_1, f_0 and f_2 at the drop port were 1.065, 2.160, and 3.217 GHz. The coupling coefficients were −17.190, −16.115, and −14.657 dB, accordingly. The

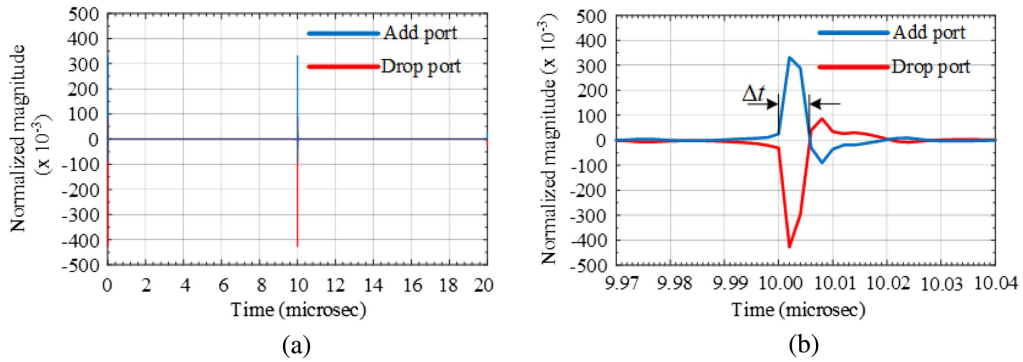

Fig. 6. Simulation of the time domain of (a) normal and (b) zoom signals of the Rabi antenna. The electrons are split into two sides of time. The blue-shift on the right side has occurred with the electron time dilation, which will collapse and be returned to the origin.

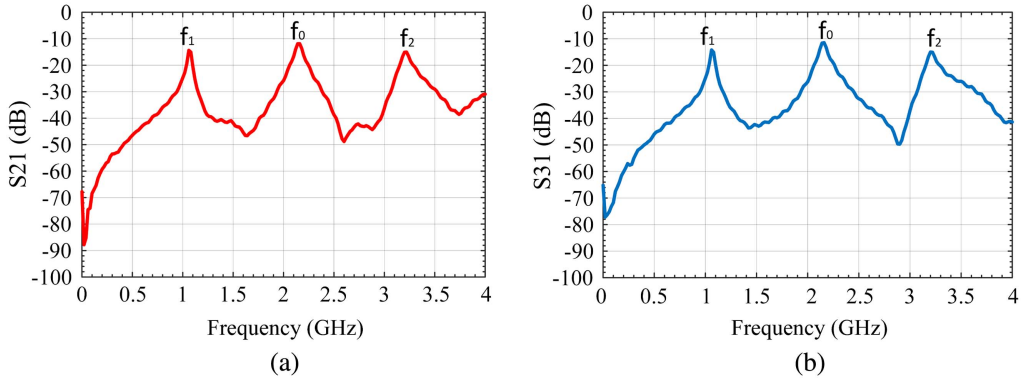

Fig. 7. Measurement of magnitude of (a) S_{21} and (b) S_{31} of the Rabi antenna.

measurement results at add-port response frequencies of f_1, f_0, f_2 and the coupling coefficients were 1.065, 2.160, 3.217 GHz and −21.789, −15.948, −14.671 dB, as shown in Fig. 7(b), respectively. The frequency differences of f_0–f_2, f_0–f_1, and f_2–f_1 are 1.033, 1.063 and 2.096 GHz, respectively. In Fig. 8(a), the response frequencies of f_1, f_0, f_2 and the connection coefficients (magnitude, coupling factor) of the drop port are 1.065, 2.160, 3.217 GHz and 0.190, 0.256, 0.178. Considering the measurements at the add port (isolation port), the response frequencies of response f_1, f_0 and f_2 and the normalized magnitudes of S_{31} are 1.095, 2.160, 3.217 GHz and 0.190, 0.267, 0.176, as shown in Fig. 8(b), respectively. The frequency differences f_0–f_1, f_2–f_0, f_2–f_1 are 1.065, 0.967, 2.152 GHz, respectively. Finally, Fig. 9 (a) shows the real part of the drop-port results ranging from −0.25 to 2.5, while Fig. 9(b) shows the real part of the add port ranging from−0.18 to 0.18 to the various frequencies.

In application, the use of the relativistic behaviors of photons (electrons) within the transition energy gap to form the travelling speed faster than light speed can be realized before the system collapses. The electrons moving in the circuit faster than light speed can be confirmed by the blue-shift and travelling speed calculation ($v = 2\pi f r$). The two-level energy gap is

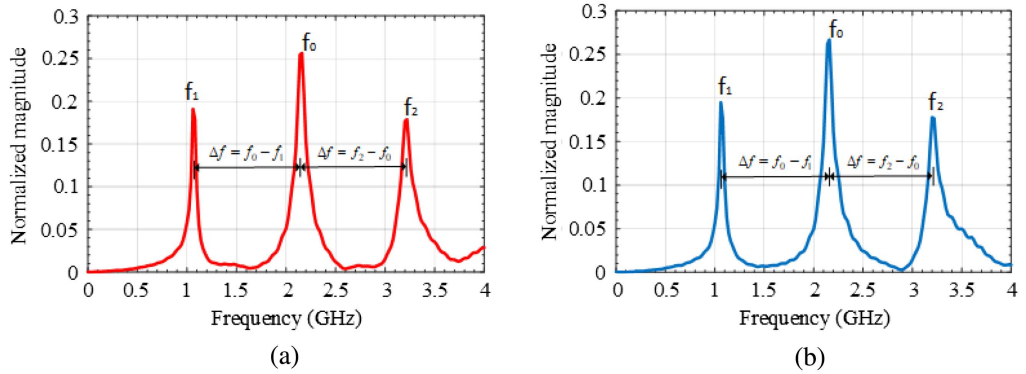

Fig. 8. Measurement of magnitude of (a) S_{21} and (b) S_{31} of the Rabi antenna.

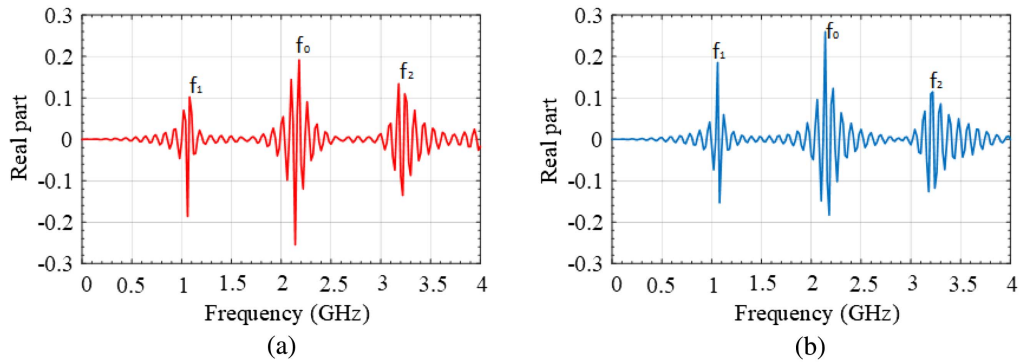

Fig. 9. Real part measurements at (a) the drop port and (b) the add port responses f_1, f_0, and f_2 are 1.065, 2.160, and 3.217 GHz.

decreased during the blue-shift process, from which the electron speed faster than light speed (warp speed)[31] can be achieved. Moreover, when the two-level states from the two different spaces (ports) are overlapped, the same signals can be detected at the orthogonal detectors. The two spaces can be connected and teleport electrons (information). Finally, the two energy states are collapsed, which means the system has gone to the singularity, where the wormhole is formed. For further applications, the wireless photon (electron) transmission using the Rabi antenna can be applied. The Rabi orthogonal energy modes of the excited and ground states can be detected randomly via the similar output device ports. Thus, the up-link and down-link transmission of the quantum information can be applied for quantum computers and communication. Besides, the Rabi antenna is also available for quantum sensors, which can be used.

4. Conclusion

We have demonstrated that the Rabi oscillation of the two-level system can be formed by the driven AC into a microstrip add-drop multiplexer. The AC coupling power into the circuit can drive electrons moving along the device structure, where initially the multi-level system of electron oscillation is formed based on the wave-particle duality aspect. The higher-order modes of multi-level system oscillation are filtered by successive filtering, from which the resonant Rabi oscillation is obtained. From the experiment, the obtained center frequency is at 2.103 GHz, which is resonant with the FR4 microstrip ring radius of 25 mm and the input AC frequency of 4 GHz. Consequently, the blue-shift of the Rabi oscillation is observed with the frequency of 2.160 GHz, from which the calculated electron warp speed of 1.10c is achieved, and the time dilation is 6 ns. Most of the obtained results have shown good agreement with the simulation. However, there are deviations from the simulation, which may be caused by the device construction errors. The designed Rabi antenna can be applied for both electronic circuits and antenna usages, from which the quantum operation using the circuit can be used. Moreover, the sub-level sensors using the suitable arrangement for cells, molecules, atoms, and spectroscopy can be realized. The connection between two spaces (device ports) can be observed before collapsing. It has the possibility of using the teleport channel for electron transportation, where the same electrons can appear in different spaces. Using this device structure, the larger ring radius can be made with suitable material and AC driven frequency, which can offer more aspects of investigations. There are also some curious aspects of the gap of the Rabi oscillation transition states during successive filtering that can be focused for future investigations.

Acknowledgement

The authors acknowledge research facility support from the Institute of Vocational Education Northeastern Region 2, Sakon Nakhon and Nakhon Phanom University, Nakhon Phanom, Thailand.

References

1. F. Assemat, D. Grosso, A. Signoles, A. Facon, I. Dotsenko, S. Haroche, J. Raimond, M. Brune, and S. Gleyzes, "Quantum Rabi oscillations in coherent and in mesoscopic cat field states," Phys. Rev. Lett. **123**, 143605 (2019).
2. L. Zhang, Y. Zhang, Y. Yang, and H. Chen, "Experimental study of Rabi-type oscillation induced by tunneling modes in effective near-zero-index metamaterials," Phys. Rev. E **83**, 046604 (2011).
3. H. Kamada, H. Gotoh, J. Temmyo, T. Takagahara, and H. Ando, "Exciton Rabi oscillation in a single quantum dot," Phys. Rev. Lett. **87**, 246401 (2001).
4. K. A. Fischer, L. Hanschke, J. Wierzbowski, T. Simmet, C. Dory, J. J. Finley, J. Vučković, and K. Müller, "Signatures of two-photon pulses from a quantum two-level system," Nat. Phys. **13**, 649 (2017).
5. M. Brune, F. Schmidt-Kaler, A. Maali, J. Dreyer, E. Hagley, J. Raimond, and S. Haroche, "Quantum Rabi oscillation: a direct test of field quantization in a cavity," Phys. Rev. Lett. **76**, 1800 (1996).
6. L. Chen, G.-W. Zhang, C.-L. Bian, C.-H. Yuan, Z. Ou, and W. Zhang, "Observation of the Rabi oscillation of light driven by an atomic spin wave," Phys. Rev. Lett. **105**, 133603 (2010).
7. C. Law, "Vacuum Rabi oscillation induced by virtual photons in the ultrastrong-coupling regime," Phys. Rev. A **87**, 045804 (2013).
8. D. Wang, H. Kelkar, D. Martin-Cano, D. Rattenbacher, A. Shkarin, T. Utikal, S. Götzinger, and V. Sandoghdar, "Turning a molecule into a coherent two-level quantum system," Nat. Phys. **15**, 483 (2019).
9. J.-L. Wu, S.-L. Su, Y. Wang, J. Song, Y. Xia, and Y.-Y. Jiang, "Effective Rabi dynamics of Rydberg atoms and robust high-fidelity quantum gates with a resonant amplitude-modulation field," Opt. Lett. **45**, 1200 (2020).
10. H. Zhong, Y. V. Kartashov, Y. Zhang, D. Song, Y. Zhang, F. Li, and Z. Chen, "Rabi-like oscillation of photonic topological valley Hall edge states," Opt. Lett. **44**, 3342 (2019).
11. F. Raza, A. Imran, X. Li, W. Li, Y. Li, J. Mao, and Y. Zhang, "Multi-mode correlation with self-and cross-Rabi oscillation in a diamond nitrogen-vacancy center," Laser Phys. Lett. **16**, 055402 (2019).
12. T. Chen, K. Shibata, Y. Eto, T. Hirano, and H. Saito, "Faraday patterns generated by Rabi oscillation in a binary Bose–Einstein condensate," Phys. Rev. A **100**, 063610 (2019).
13. K. Kuruma, Y. Ota, M. Kakuda, S. Iwamoto, and Y. Arakawa, "Time-resolved vacuum Rabi oscillations in a quantum-dot–nanocavity system," Phys. Rev. B **97**, 235448 (2018).
14. V. Gudmundsson, H. Gestsson, N. R. Abdullah, C.-S. Tang, A. Manolescu, and V. Moldoveanu, "Coexisting spin and Rabi oscillations at intermediate time regimes in electron transport through a photon cavity," Beilstein J. Nanotechnol. **10**, 606 (2019).
15. S. Soysouvanh, M. Jalil, I. Amiri, J. Ali, G. Singh, S. Mitatha, P. Yupapin, K. Grattan, and M. Yoshida, "Ultra-fast electro-optic switching control using a soliton pulse within a modified add-drop multiplexer," Microsyst. Technol. **24**, 3777 (2018).
16. S. Wang, X. Feng, S. Gao, Y. Shi, T. Dai, H. Yu, H.-K. Tsang, and D. Dai, "On-chip reconfigurable optical add-drop multiplexer for hybrid wavelength/mode-division-multiplexing systems," Opt. Lett. **42**, 2802 (2017).
17. B. Naghdi and L. R. Chen, "Silicon photonic four-channel optical add-drop multiplexer enabled by subwavelength grating waveguides," IEEE Photonics J. **10**, 6601510 (2018).
18. M. G. Saber, Z. Xing, D. Patel, E. El-Fiky, N. Abadia, Y. Wang, M. Jacques, M. Morsy-Osman, and D. V. Plant, "A CMOS compatible ultracompact silicon photonic optical add-drop multiplexer with misaligned sidewall Bragg gratings," IEEE Photonics J. **9**, 6601010 (2017).
19. S. Wang, H. Wu, H. K. Tsang, and D. Dai, "Monolithically integrated reconfigurable add-drop multiplexer for mode-division-multiplexing systems," Opt. Lett. **41**, 5298 (2016).
20. D. Wu, Y. Wu, Y. Wang, J. An, and X. Hu, "Reconfigurable optical add-drop multiplexer based on thermally tunable micro-ring resonators," Opt. Commun. **367**, 44 (2016).

21. D. A. B. Miller, "Reconfigurable add-drop multiplexer for spatial modes," Opt. Express **21**, 20220 (2013).
22. X. Xiao, X. Li, X. Feng, K. Cui, F. Liu, and Y. Huang, "Eight-channel optical add-drop multiplexer with cascaded parent-sub microring resonators," IEEE Photonics J. **7**, 7801307 (2015).
23. A. Kato, K. Nakatsuhara, and Y. Hayama, "Switching operation in tunable add-drop multiplexer with Si-grating waveguides featuring ferroelectric liquid crystal cladding," J. Lightwave Technol. **32**, 4464 (2014).
24. M.-Y. Chen and J. Zhou, "Design of add-drop multiplexer based on multi-core optical fibers for mode-division multiplexing," Opt. Express **22**, 1440 (2014).
25. D. Pérez-Galacho, D. Marris-Morini, A. Ortega-Moñux, J. Wangüemert-Pérez, and L. Vivien, "Add/drop mode-division multiplexer based on a Mach–Zehnder interferometer and periodic waveguides," IEEE Photonics J. **7**, 7800907 (2015).
26. S. Sonasang and N. Angkawisittpan, "Design of microstrip parallel-coupled lines with high directivity using symmetric-centered inductors," ACES Journal **36**, 657 (2021).
27. C. A. Balanis, *Antenna Theory: Analysis and Design* (Wiley, 2016).
28. A. Garhwal, A. E. Arumona, P. Youplao, K. Ray, I. S. Amiri, and P. Yupapin, "Human-like stereo sensors using plasmonic antenna embedded MZI with space–time modulation control," Chin. Opt. Lett. **19**, 101301 (2021).
29. P. Phatharacorn, S. Chiangga, and P. Yupapin, "Analytical and simulation results of a triple micro whispering gallery mode probe system for a 3D blood flow rate sensor," Appl. Opt. **55**, 9504 (2016).
30. M. Frimmer and L. Novotny, "The classical Bloch equations," Am. J. Phys. **82**, 947 (2014).
31. A. Garhwal, A. E. Arumona, K. Ray, P. Youplao, S. Suwandee, and P. Yupapin, "Microplasma source circuit using microring space–time distortion control," IEEE Trans. Plasma Sci. **48**, 3600 (2020).